Journal of Building Engineering 112 (2025) 113893

Contents lists available at ScienceDirect

Journal of Building Engineering

journal homepage: www.elsevier.com/locate/jobe

Comparative study on flexural characteristics of dry ultra-high performance concrete with mono and hybrid steel fibre reinforcement

Chaocong Wang [a], Ruizhe Shao [a,*], Jianguang Fang [a], Jun Li [a], Chengqing Wu [b,a,**]

[a] School of Civil and Environmental Engineering, University of Technology Sydney, Sydney, NSW, 2007, Australia
[b] Institute of Rock and Soil Mechanics, Chinese Academy of Sciences, Wuhan, 430071, China

ARTICLE INFO

Keywords:
Dry UHPC (DUHPC)
Fibre reinforcement
Flexural characteristic
Digital image correlation (DIC)
Scanning electron microscope (SEM)

ABSTRACT

Dry ultra-high performance concrete (DUHPC) is a novel construction material that merges the properties of traditional dry concrete with UHPC, combining the advantages of both to offer superior early and long-term strength, enhanced ductility, and improved sustainability. This study investigated the flexural behaviour of DUHPC reinforced with mono and hybrid steel fibres. The evaluation focused on the load-crack mouth opening displacement (CMOD) relationship, flexural strength, initial fracture toughness, unstable fracture toughness, and fracture energy. The mono fibre contents ranged from 0.5% to 1.5%, utilizing fibres of 10 mm and 13 mm in length. For hybrid fibre reinforcement, the total fibre content maintained at 1.5%, consisting of 10 mm and 13 mm steel fibres. Experimental results showed that the addition of steel fibres significantly enhanced the flexural behaviour of DUHPC as compared to the control group. After 28 days of curing, the flexural strength demonstrated an increase of up to 401.3% relative to the control group, with fracture energy reaching 39.2 kJ/m^2. Hybrid fibres exhibited varied toughening effects; the replacement of 13 mm fibres with 10 mm ones led to the reductions in flexural strength and fracture energy, while the initial fracture toughness increased by 3.9% and the unstable fracture toughness increased by 2.1%. Digital image correlation (DIC) images corroborated the superior strength and toughening effects of longer steel fibres. Moreover, scanning electron microscope (SEM) micrographs showcased the dense microstructure of DUHPC post moist/steam curing. The embedded fibres markedly improved the material's resistance to bending loads through the synergistic effects of fibre deformation, pull-out, and interfacial friction, thus enhancing the overall flexural performance of DUHPC.

1. Introduction

Concrete has become a mainstream building material owing to its wide range of raw material availability, low cost, simple production process, and good fire resistance. Concrete mixtures can be divided into fluid and non-fluid types. Dry concrete, with a slump usually not more than 25 mm, lacks fluidity after mixing [1,2]. Dry concrete often includes alternative supplementary cementitious materials (ASCMs) and a high aggregate-cement ratio relative to self-compacting concrete, allowing for fast setting, rapid demoulding

* Corresponding author. School of Civil and Environmental Engineering, University of Technology Sydney, NSW, 2007, Australia.
** Corresponding author. Institute of Rock and Soil Mechanics, Chinese Academy of Sciences, Wuhan, 430071, China.
E-mail addresses: Ruizhe.shao@uts.edu.au (R. Shao), cqwu@whrsm.ca.cn (C. Wu).

https://doi.org/10.1016/j.jobe.2025.113893
Received 13 April 2025; Received in revised form 28 July 2025; Accepted 23 August 2025
Available online 24 August 2025

and cost effectiveness [3–5]. Dry concrete is broadly classified into two types, roller-compacted concrete (RCC) [6] and dry-cast concrete (DCC) [7], which differ in their mix proportions, water content, and applications. RCC, with a low water-cement ratio, is utilized in high-strength applications like paving and dams, using bulldozers and vibrating rollers for compaction [8,9]. DCC, with an even drier mix, is used in concrete masonry and precast units as well as roof tiles, allowing for rapid demoulding and highlighting concrete adaptability for specific construction and manufacturing needs [10].

Shao et al. [11] pointed out that dry concrete possesses a high volume of ASCMs, which affects its properties to a certain extent. For example, when 0–60% fly ash (FA) was used to replace part of the cement, the strength of RCC decreased with increasing FA content, and the influence on early strength was especially obvious. Ramezanianpour et al. [12] and Ghahari et al. [13] further noted that when Trass was used to substitute part of cement, it also led to some loss of strength at an early stage. This resulted from the low pozzolanic activity of Trass, which may not be beneficial for hydration in the early periods. Therefore, to mitigate the degradation of mechanical properties due to ASCM inclusion, adding fibres to dry concrete matrix is one of the effective methods.

Specifically, fibres can inhibit shrinkage-induced micro-cracking and slow down the expansion in the early stage. They act as a bridge in concrete matrix, effectively delaying the development of cracks and enhancing the crack resistance of the material. Additionally, fibre reinforcement reduces the risk of expansion-related cracks by controlling the moisture movement and thermal volume changes [14–17]. Rooholamini et al. [18] and Karadelis et al. [19] have demonstrated that incorporating fibres into dry concrete can increase the fibre effectiveness. This is mainly because the internal structure of dry concrete is much denser than conventional concrete and the interaction between the fibres and the matrix is thus increased. Sukontasukkul et al. [20] investigated the difference in mechanical properties between RCC pavement (RCCP) and steel fibre-reinforced RCCP. Steel fibre-reinforced RCCP exhibited higher modulus of rupture and flexural toughness. With an addition of 1% hooked end steel fibres, the modulus of rupture increased from 4.1 MPa to 5.0 MPa, and the flexural toughness was 19 times higher when compared to that of the RCCP without fibres. LaHucik et al. [21] utilized six (four synthetic and two steel) different fibres to reinforce RCC and discussed the variations in mechanical properties. The addition of five types of fibres proved to be effective in enhancing both the compressive and splitting tensile strengths when compared to the control group. Only high carbon steel fibres showed a reduction in compressive strength. From the 28-day compressive test, it was observed that the compressive strength of specimens with 0.4% polypropylene fibres increased from 46.7 MPa to 56.6 MPa, and those with 0.2% steel fibres demonstrated the highest splitting tensile strength gain, from 4.0 MPa to 6.8 MPa. Sharbatdar et al. [22] also used varying types of fibres to reinforce RCCP. When 0.27% steel fibres were included, the compressive and flexural strengths were the highest among the four fibres (steel, Sinusoidal plastic, Kortta Emboss, and Kortta Twist), reaching 60.3 MPa and 6.2 MPa, respectively. For the Brazilian tensile test, the specimen with 0.27% Kortta emboss fibres exhibited the most significant improvement. Fracture behaviour of RCCP with mono and hybrid fibres was tested by Scorza et al. [23]. For the mono fibre reinforcement, specimens with 0.7% steel fibres (35 mm) exhibited the optimal results regarding peak load and fracture toughness, which were 2.1 kN and 1.0 MPa$\sqrt{\text{m}}$, respectively. For the hybrid fibre reinforcement, the above properties were generally intermediate between the two mono fibre groups. Moreover, Liang et al. [24] studied the effect of multi-scale polypropylene fibre (PPF) on RCCP reinforcement after 3–28 days of curing. The microscale PPFs primarily enhanced the mechanical performance of RCCP during the early curing stage (within 7 days). However, after 7 days, the macroscale PPFs played a dominant role by bridging the larger cracks. The study likewise indicated that the multi-scale RCCP performed best in terms of compressive and tensile strength. The 28-day splitting tensile strength could reach 5.5 MPa and the compressive strength was 67 MPa. As reviewed above, although the addition of various fibres has enhanced the mechanical behaviour of dry concrete, they are still insufficient to meet the stringent requirements of modern construction, including enhanced mechanical strength, improved crack resistance, reduced construction time, cost-effectiveness, and sustainability. Therefore, a new type of building material is needed that is more powerful and more reliable.

The progress of ultra-high performance concrete (UHPC) provides the construction industry a material with higher compressive strength and better ductility, achieved by incorporating fibres and optimizing granules with ultrafine particles [25]. UHPC typically possesses compressive strength above 120.0 MPa, and its flexural strength can reach up to 40.0 MPa [26–28]. In this context, leveraging the advantages of UHPC to develop a novel form of dry UHPC (DUHPC) appears to be highly promising. DUHPC integrates the qualities of both concretes, delivering high early and long-term strength, great ductility, and cost-effective production.

Steel fibre-reinforced DUHPC's mechanical properties were initially established by Shao et al. [29]. It was concluded that all the DUHPC's strengths increased with steel fibre content (0.5%–2.0%). The compressive, flexural, and splitting tensile strengths at 28 days could reach up to 168.9 MPa, 36.6 MPa, and 14.2 MPa, respectively, which were 76.7%, 125.9%, and 105.8% higher than the control group. It was also concluded that wet-steamed curing at 50 °C was most suitable for the consolidation of DUHPC through different curing methods. Additionally, Shao et al. [30] examined how the high-volume FA and waste rubber particles affected DUHPC. A notable reduction in both compressive and flexural strengths was observed as the content of FA increased, especially for specimens with higher FA content in the early stages. Specifically, the compressive strength decreased from 134 MPa to 94.7 MPa and the flexural strength decreased from 33.2 MPa to 24.8 MPa as the FA content increased from 20% to 60%. Moreover, the study highlighted the environmental benefits, such as reduced sand usage and enhanced recycling of waste materials. Economically, increasing FA addition from 20% to 60% lowered the total cost from 279.6 CNY to 107.5 CNY per volume unit, and utilizing rubber particles as the aggregates proved more cost-effective as compared to steel fibre reinforcement.

Significant progress has been made in the mechanical strength of DUHPC, but there are still unexplored areas in key performance indicators. Therefore, further exploring the behaviour of DUHPC in terms of fracture toughness and energy absorption properties will not only help to gain a deep understanding of the material but also provide theoretical support for its real-world application in structures.

2. Material selection, mix design, and preparation

2.1. Raw material composition and proportions

The main materials used to prepare DUHPC included Portland cement (42.5N, Type GP), silica fume, FA, ground granulated blast-furnace slag (GGBS), sand, steel fibre, polycarboxylate superplasticizer (SP), and water. FA, silica fume, and GGBS were utilized as ASCMs and their main function was to replace partial cement. Using ASCM as a cement substitute lowers CO_2 emissions, conserves non-renewable resources, reduces waste, and improves concrete mixture performance. The water-to-binder ratio was fixed as 0.16, in accordance with the findings of a previous study [31]. Table 1 provides a detailed summary of chemical compositions of cement, silica fume, FA, and GGBS.

Two lengths of copper-coated steel fibres (effective protection against environmental corrosion, shown in Fig. 1) measuring 10 and 13 mm in length and 0.12 mm in diameter were selected. Polycarboxylate SP containing early-strength ingredients (naphthalene sulfonate formaldehyde condensate) was added to the mixture, which gave a better early behaviour of DUHPC. Two steel fibre mixtures as presented in Table 2 below were used to assess the influence related to multiscale mono/hybrid fibres regarding the flexural characteristics of DUHPC. In mono fibre reinforcement, the volume fraction was 0.5%, 1.0%, and 1.5%. In hybrid fibres, two blends were used, maintaining the total volume content at 1.5%, which Shao et al. [29] identified as the optimal fibre content for DUHPC. When the fibre content exceeded 1.5%, it led to fibre agglomeration that adversely affected performance. Table 2 shows the details of the mixture proportions for mono and hybrid DUHPC. To identify different specimens, 0.5, 1.0, and 1.5 represent the fibre volume fraction for the mixture, S (10 mm) and L (13 mm) represent the length of the fibres. For example, S0.5 denotes the mixture incorporating 0.5% volume addition with 10 mm steel fibres. Fibre-free specimens were also fabricated as the control group.

2.2. Preparation and curing method

The preparation process had different steps attributable to the decreased moisture content in DUHPC. The processes were roughly divided into the following steps: (1) Mix weighed dry ingredients. The speed of the mixer was 60 revolutions per minute and mixing was done at this speed for 2 min (2) Disperse steel fibres and add them to the mixer slowly and uniformly to achieve better later results and continue mixing for 4 min (3) Add the SP solution mixed in advance, following by evenly pouring the solution into the mixer, and then stirring for 5 min (4) Pour three layers for each specimen due to the characteristics of DUHPC. After each layer was cast, it was compacted and then put into the laboratory vibrating table to achieve the final shape. This process was conducted three times. Fig. 2 shows the detailed procedure of the preparation process.

Using early high-temperature curing is an effective strategy to expedite DUHPC solidification and improve early performance [31]. After casting, specimens were first placed in a constant temperature and humidity chamber to minimise external interference. After all the specimens have been poured, the specimens were placed in a 50 °C curing chamber. The specimen steam cured for 24 h. After steam curing, the specimens were demoulded and labelled, following by placing them in a thermostatic water tank for 13 and 27 days as required for the experiment. The specimens had dimensions of 40 mm × 40 mm × 160 mm. A total of 9 groups of specimens were prepared, including 6 groups of mono fibre-reinforced DUHPC, 2 groups of hybrid fibre-reinforced DUHPC, and 1 control group without fibre reinforcement. Each group contained 3 prisms for each testing age, resulting in a total of 54 DUHPC specimens. The bending testing procedure followed the specifications of ASTM C293/C293M, which specifies the method for evaluating the flexural behaviour of concrete using centre-point loading. Since the specimens will be subjected to the three-point bending, an opening mouth in the middle of the prism is required. To achieve this, notches with an opening mouth and depth of 5 mm were created by marking the centre line on the bottom surface, followed by the controlled grooving and precise sawing to ensure uniformity [32]. Fig. 3 presents the fabricated specimens for the three-point bending test.

3. Testing program

The testing apparatus should be calibrated to apply load at the two upper loading points, while the beam was supported at its ends. The specimen was fixed on the testing machine in such a way that the notch was facing downwards, while the load was applied on the opposite face. The loading rate should be carefully controlled to maintain a stable crack propagation, and the load and mid-span deflection are continuously monitored throughout the test. Firstly, the marked specimens were placed on the rack as needed,

Table 1
Chemical compositions of cement, silica fume, FA, and GGBS.

Components/Properties (%)	Cement	Fly ash	Slag	Silica fume
CaO	64.5	1.3	40.5	0.2
SiO_2	21.0	65.2	35.4	98.5
Al_2O_3	5.2	26.0	13.0	0.2
Fe_2O_3	3.2	3.1	0.4	0.1
MgO	1.2	0.7	8.0	0.5
TiO_2	–	1.1	0.5	0.1
SO_3	2.2	0.2	0.5	0.1
K_2O	0.3	1.7	–	0.2

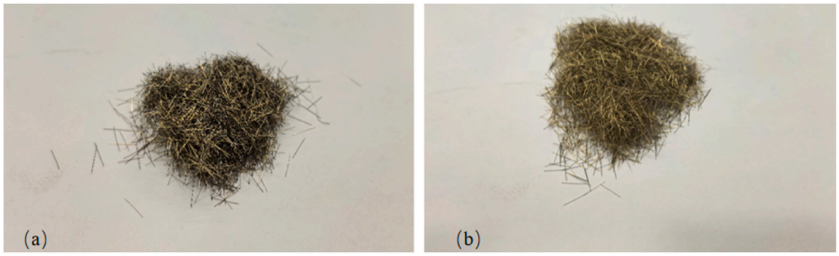

Fig. 1. Copper-coated steel fibres used in this study: (a) 10 mm and (b) 13 mm in length.

Table 2
Mixture proportions of DUHPC by weight.

Fibre type	Cement	Silica fume	FA	GGBS	Sand	Water	SP	Fibre (vol%)	Fibre proportions
Non-fibre	1.00	0.15	0.31	0.08	2.84	0.25	0.03	0	Control
Mono	1.00	0.15	0.31	0.08	2.84	0.25	0.03	0.5, 1.0, 1.5	S0.5-S1.5, L0.5-L1.5
Hybrid	1.00	0.15	0.31	0.08	2.84	0.25	0.03	1.5	S1.0L0.5, S0.5L1.0

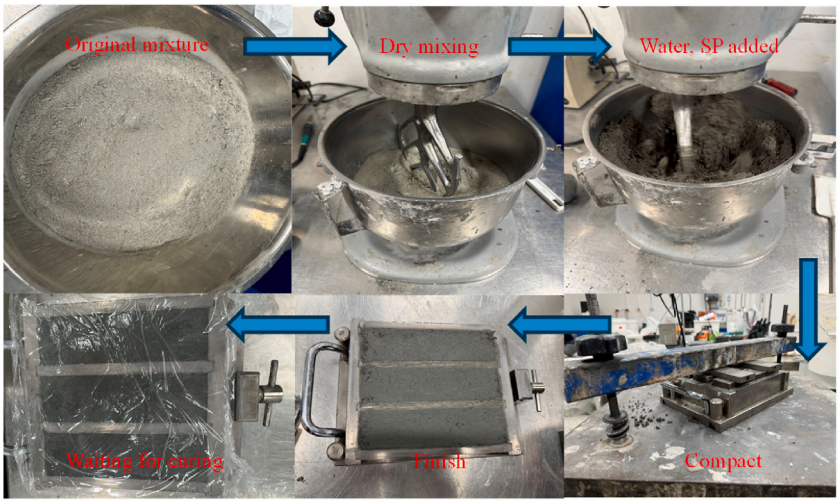

Fig. 2. Preparation process of DUHPC bending specimens.

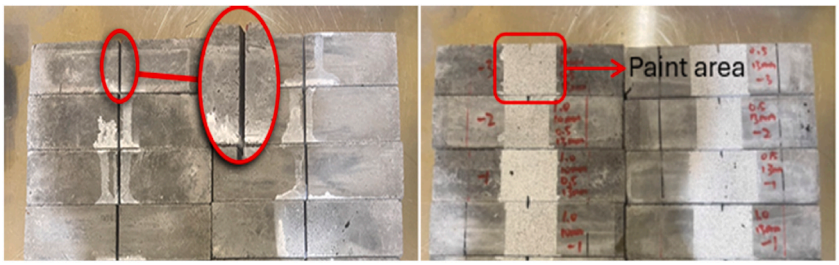

Fig. 3. Fabricated specimens for three-point bending test.

where must ensure the accuracy of the specimen placement. Then a loading pin was fixed directly above the specimen with a stroke of 0.2 mm/min.

DIC technology, a non-contact optical measurement method, was used to observe displacement, strain distribution, and crack initiation/propagation at mid-span and the opening mouth. Before the test started, the specimen's smoother surface, characterized by a reduced number of voids, was selected as the test surface for DIC. Subsequently, the measurement area of the specimen was coated with matte paint. When the specimens were ready, as shown in Fig. 4, a camera was installed in front of the test machine to ensure that the

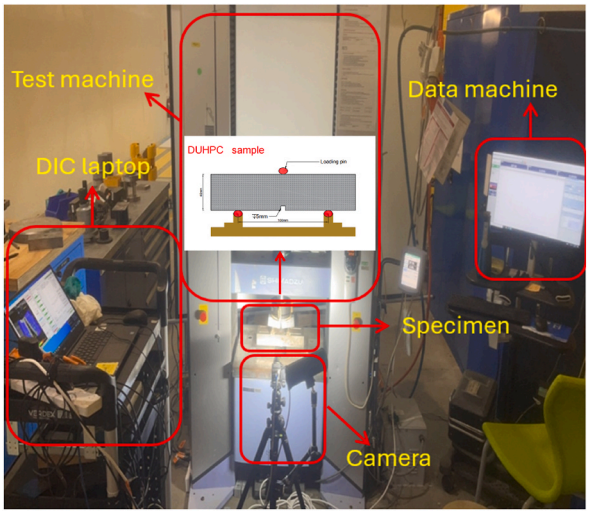

Fig. 4. Three-point bending test setup with DIC assistance.

camera accurately confronted the measurement zone of the three-point bending specimen. Since the experiment was conducted indoors, spotlights were placed on right hand sides of the machine to adjust the fill light in order to ensure that the shooting effect was not affected by the dark environment. To gather a sufficient number of images and the failure modes observed during testing, the camera was acquired at a frequency of 10 Hz in accordance with the testing requirements.

4. Results and discussion

4.1. Load-CMOD relationship

The effect of fibre content and length on the load-crack mouth opening displacement (CMOD) relationship is vital for understanding the crack propagation behaviour of DUHPC. Fig. 5(a and b) illustrate the typical load-CMOD curves for specimens reinforced with 10 mm and 13 mm steel fibres, respectively. Without considering the fibre length, the peak load increased when the fibre content increased. As an illustration, when the fibre content increased from 0.5% to 1.5%, the peak load of the 10 mm fibre specimens increased from 3.2 kN to 8.8 kN, indicating an increase of 175.0%. Under the same conditions, for 13 mm fibres, the peak load increased from 3.9 kN to 11.8 kN, exhibiting a remarkable improvement of 202.0%. Additionally, the increase in fibre content helped delay CMOD expansion. For example, when the CMOD reached 6 mm, specimens reinforced with 10 mm steel fibres exhibited a residual load of 0.6 kN at a fibre content of 0.5%. When the fibre content increased to 1.0%, the residual load increased to 1.2 kN, and the best residual load was observed at a fibre content of 1.5%, yielding 2.6 kN. This is predominantly due to the increased fibre content, which results in a denser and more uniform fibre distribution within the concrete matrix, forming an effective fibre network that enhances load capacity and limits crack propagation [33].

The peak load of 13 mm steel fibre-reinforced DUHPC consistently exceeded 10 mm fibre-reinforced counterparts at all content levels. This difference is evident from the comparison between Fig. 5(a and b). With a steel fibre content of 1.5%, the peak load for the 13 mm fibres reached 11.8 kN, whereas the 10 mm fibres was only 8.8 kN, representing a reduction of 25.4%. Regarding CMOD, the 13 mm fibres also proved more effective in delaying CMOD expansion. For instance, when the CMOD reached 6 mm, the residual load for the 13 mm fibre-reinforced specimen was 36.4% of its peak load, while for the 10 mm fibre-reinforced counterpart, it was only 29.5%. This enhancement can be attributed to the greater anchorage length of the longer steel fibres, allowing for more effective crack bridging and thus significantly delaying crack propagation.

Fig. 5(c) presents the load-CMOD curves for hybrid fibres. It can be observed that the peak load of the two hybrid fibre groups showed minimal variation, with the value of the S1.0L0.5 specimen only 6.3% lower than the L1.5 case. Regarding the CMOD, when it expanded to 6 mm, the residual load of the S0.5L1.0 specimen reached 29.4% of its peak load, while that of the S1.0L0.5 was approximately 19.8%. Additionally, in the descending phase of these curves, a distinct fluctuation phase can be observed. This is primarily attributed to the shorter steel fibres being progressively pulled out, while the longer fibres continue to bridge the cracks, maintaining their anchorage and providing sustained crack bridging ability. For the hybrid fibre-reinforced specimens, the peak load was generally intermediate between those of the mono fibre-reinforced specimens S1.5 and L1.5, both having the same total fibre content of 1.5%. As mentioned in Introduction, DUHPC differs from the self-compacting concrete, featuring a very low water-to-binder ratio, which results in a dry mixture appearance. Hence, when selecting fibre lengths, it is essential to consider not only their contribution to mechanical performance but also their effect on the workability of DUHPC. Studies reveal that longer fibres negatively impact the workability of both dry and self-compacting concretes [23,31,34]. Consequently, the S0.5L1.0 mix may offer better overall performance as compared to L1.5 mix.

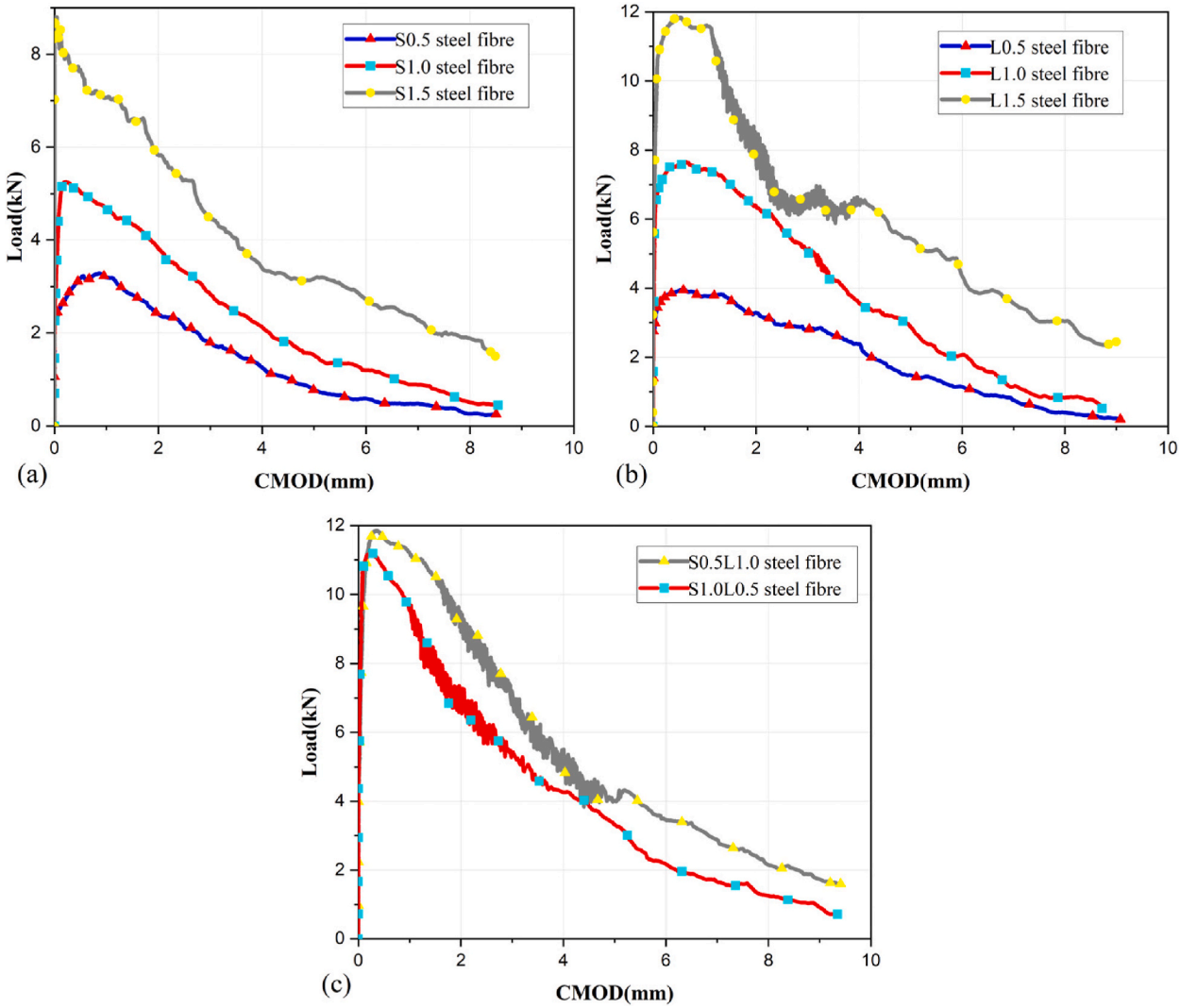

Fig. 5. Typical load-CMOD relationships of (a) 10 mm, (b) 13 mm, and (c) hybrid steel fibre-reinforced DUHPC.

4.2. Flexural strength

Flexural strength is a key mechanical property used to evaluate the resistance of materials to bending deformation. The flexural strength of DUHPC is calculated by using Eq. (1):

$$f = \frac{3PL}{2bh^2} \tag{1}$$

where f denotes the flexural strength; P denotes the peak load to which the specimen is subjected; L represents the span length of the testing beam; b is referred to as the width of the beam; h refers to the height of specimen minus the depth of the opening mouth. Fig. 6 illustrate the effects of varying fibre content, length, and combination methods on the flexural strength of DUHPC. Combined with Table 3, which presents the strength values and their growth rate relative to the control group, it was observed that the flexural strength of mono steel fibre-reinforced DUHPC specimens increased significantly with fibre content and length. For instance, the 14-day flexural strength of specimen S0.5 was 9.1 MPa, an increase of 93.6% as compared to the control case's 4.7 MPa. Similarly, specimen S1.5 achieved a 14-day flexural strength of 16.0 MPa, with a growth rate of 240.4%. At 28 days, this trend became even more pronounced, with specimen S1.5 reaching a flexural strength of 26.9 MPa, marking an increase of 273.6% in comparison with the control group. As described in Section 4.1, this significant improvement was primarily attributed to the increased fibre content, which resulted in a denser fibre distribution within the DUHPC matrix, thereby enhancing crack control and improving flexural performance [35].

Fibre length also had a significant impact on flexural strength of DUHPC. Specimens with 13 mm steel fibres exhibited greater

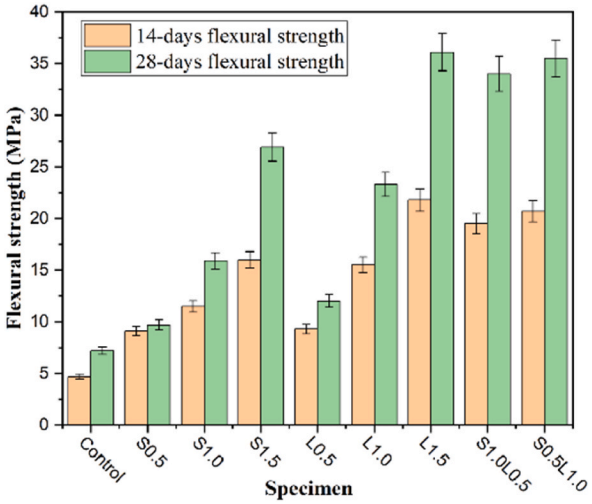

Fig. 6. Flexural strength of DUHPC with 10 mm and 13 mm steel fibres.

Table 3
Flexural strength and growth rate of DUHPC.

Specimen	14 days (MPa)	Rate (%)	28 days (MPa)	Rate (%)
Control	4.7	–	7.2	–
S0.5	9.1	93.6	9.7	34.7
S1.0	11.5	144.6	15.9	120.8
S1.5	16.0	240.4	26.9	273.6
L0.5	9.3	97.8	12.0	66.6
L1.0	15.5	229.7	23.3	223.6
L1.5	21.8	363.8	36.1	401.3
S1.0L0.5	19.5	314.8	34.0	372.2
S0.5L1.0	20.7	340.4	35.5	393.1

flexural strength when compared to those with 10 mm fibres. At 14 days, specimen S1.0 achieved a flexural strength of 11.5 MPa, while specimen L1.0 reached 15.5 MPa, reflecting a 34.8% increase. At 28 days, the flexural strength of specimen L1.0 increased to 23.3 MPa, an increase of 46.5% as compared to specimen S1.0. This indicated that 13 mm steel fibres were proved to be more effective in improving the bending performance of DUHPC. This improvement can be mainly attributed to the increased bond area between the longer fibres and the matrix, requiring greater pull-out energy to extract the fibres from the matrix [36]. Additionally, as mentioned in Section 2.2, the layered vibrated-compaction method utilized for casting DUHPC aligned most steel fibres with the casting plane. This orientation notably enhanced the material resistance to the bending loads [37]. Compared to the random fibre distribution in self-compacting concrete, this distinct fibre distribution inside DUHPC underscored the particular benefit of fibre length to flexural performance.

For hybrid steel fibre-reinforced DUHPC, it was observed that replacing part of the 13 mm fibres with 10 mm ones led to a decline in flexural strength. As an illustration, after 28 days of curing, the flexural strength of specimen S1.0L0.5 decreased by 5.8% relative to that of the specimen L1.5 of 36.1 MPa. However, the reduction in strength of specimen S0.5L1.0 was less pronounced, with only 1.6% compared to specimen L1.5. This was primarily due to substituted longer steel fibres with shorter ones increased the total number of fibre addition under constant fibre dosages, which resulted in a denser fibre distribution within the concrete matrix.

Table 4 summarises the flexural strength of self-compacting UHPC and DUHPC incorporating steel fibres of various lengths, types, and contents. Magureanu et al. [38] explored the influence of 25 mm steel fibres on UHPC flexural strength and reported a value up to

Table 4
Comparisons on flexural strength of steel fibre-reinforced UHPC and DUHPC.

References	Concrete	Fibre type	Length (mm)	Content (%)	f (MPa)
Magureanu et al. [38]	UHPC	Straight	25	2	~22.3
Shafieifar et al. [39]	UHPC	Straight	12.5	2	~21.9
Wu et al. [40]	UHPC	Straight, corrugated, hooked	13	1, 2, 3	~28.0
Maca et al. [41]	UHPC	Straight	13	2	~29.7
Silva et al. [42]	UHPC	Straight	13, 20	2	~30.0
This study	DUHPC	Straight	10, 13	0.5, 1.0, 1.5	~36.1

22.3 MPa when 2% fibres were used. Similarly, Shafieifar et al. [39] found that the inclusion of 2% 12.5 mm steel fibres resulted in a flexural strength up to 21.9 MPa. Wu et al. [40] prepared UHPC with straight, corrugated, and hooked steel fibre reinforcements. The specimen with 13 mm straight fibres at a content of 2% achieved a flexural strength of approximately 28.0 MPa after 28 days of curing. Maca et al. [41] and Silva et al. [42] utilized a fibre content of 2%, incorporating steel fibres with lengths of 13 mm and 20 mm, respectively. Both studies reported flexural strengths in the range of approximately 30.0 MPa.

As shown in Table 4, the flexural strength of DUHPC was significantly higher, even when the fibre content was the same or lower than that used in the aforementioned studies. Specifically, the flexural strength of the specimen with 13 mm fibres at a content of 1.5% reached 36.1 MPa. This enhancement was primarily attributed to the fibre orientation. In self-compacting concrete, steel fibres tended to be randomly dispersed, but in DUHPC, most fibres were aligned parallel to the casting surface. This alignment markedly improved the flexural performance of DUHPC.

4.3. Initial fracture toughness

The initial fracture toughness is another vital mechanical property of fibre-reinforced DUHPC, demonstrating the material's ability to resist the crack initiation and subsequent propagation, especially in the presence of pre-existing crack.

The initial fracture toughness (K_{ini}^{Ic}, MPa· $m^{1/2}$) of DUHPC in a three-point bending test is calculated by Eqs. (2) and (3) [43]:

$$K_{ini}^{Ic} = \frac{3P_{ini}S}{2D^2B}\sqrt{a_0}F\left(\frac{a_0}{D}\right) \tag{2}$$

$$F\left(\frac{a_0}{D}\right) = \frac{1.99 - (a_0/D)(1 - a_0/D)\left[2.15 - 3.93(a_0/D) + 2.7(a_0/D)^2\right]}{(1 + 2a_0/D)(1 - a_0/D)^{3/2}} \tag{3}$$

where S, D, B, and a_0 denote the span length, height, thickness, and initial crack length of the specimen (mm), respectively, $F\left(\frac{a_0}{D}\right)$ is the geometric factor, and P_{ini} is the initial crack load (N).

Fig. 7 illustrates the initial fracture toughness of steel fibre-reinforced DUHPC after 28 days of curing. It can be observed that the fracture toughness of DUHPC increased as the fibre content and length increased. For example, the initial fracture toughness of specimen S0.5 was 2.2 MPa· $m^{1/2}$, representing a 22.2% increase as compared to the control group's 1.8 MPa· $m^{1/2}$. At a fibre content of 1.0%, specimen S1.0 demonstrated a 116.6% enhancement in comparison to the control case. The greatest increase was observed at a fibre content of 1.5%, achieving a remarkable 316.6% enhancement. The increased in steel fibre content effectively enhanced the fibre quantity along the crack propagation path, inhibited the rapid development of microcracks and prevented lateral deformation of the matrix, thereby improving the fracture toughness of DUHPC. Regarding various fibre lengths, when the fibre content was 0.5%, the initial fracture toughness increased from 2.2 MPa· $m^{1/2}$ for specimen S0.5–2.5 MPa· $m^{1/2}$ for specimen L0.5, indicating a 13.6% improvement. When reaching a content of 1.0%, the toughness of specimen L1.0 improved by 56.4% as compared to specimen S1.0. At the highest content of 1.5%, 13 mm fibres contributed to a toughness value of 10.1 MPa· $m^{1/2}$, reflecting a 34.7% increase in comparison with the 10 mm ones, which was 7.5 MPa· $m^{1/2}$. This can be attributed to the longer fibres providing more effective anchoring distance across the macro-cracks, allowing the fibres to maintain continuous restraint effect even as the crack width increases, thereby enhancing the toughness performance [44].

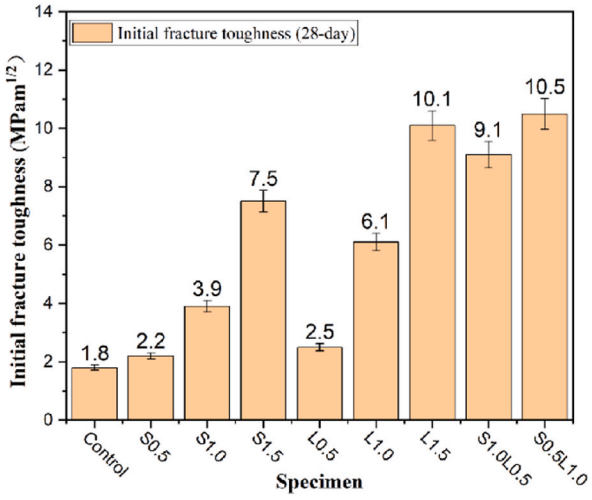

Fig. 7. Initial fracture toughness of DUHPC specimens after 28 days of curing.

For hybrid fibre-reinforced DUHPC, as mentioned in Section 4.2, the substitution of partial 13 mm steel fibres with shorter ones also influenced the initial fracture toughness. For example, the fracture toughness of specimen L1.5 was 10.1 MPa· $m^{1/2}$, while that of specimen S1.0L0.5 was 9.1 MPa· $m^{1/2}$, representing a decrease of 9.9%. But it was still higher than the initial fracture toughness of specimen S1.5. However, the fracture toughness of specimen S0.5L1.0 did not diminish, instead, it increased to 10.5 MPa· $m^{1/2}$, exhibiting a 3.9% improvement relative to L1.5. This phenomenon may be attributed to the synergistic effect of different lengths of fibres [45]. When 0.5% longer steel fibres were substituted by 10 mm ones, the reduction in fibre length led to a decrease in the mass of individual fibres, resulting in an overall increase in the number of shorter fibres. Notably, this substitution also reduced the possibility of agglomeration of longer fibres within the concrete matrix.

Based on the comparisons of the studies conducted by Cai et al. [46] and Yu et al. [47] on the initial fracture toughness of the self-compacting UHPC, it was found that although both studies employed 2% steel fibre content, the toughness was poorer than DUHPC. Specifically, Cai et al. [46] enhanced UHPC with 18 mm hooked steel fibres, achieving a maximum initial fracture toughness of 6.2 MPa· $m^{1/2}$. Yu et al. [47] studied UHPC with both straight and hooked steel fibres and found that hooked fibres outperformed straight ones. However, the toughness was only 2.3 MPa· $m^{1/2}$. In contrast, DUHPC in this study achieved significantly higher toughness values even at lower fibre contents. The specimen S0.5L1.0 yielded an initial toughness of 10.5 MPa· $m^{1/2}$.

4.4. Unstable fracture toughness

The analysis of initial fracture toughness in Section 4.3 demonstrated the resistance of DUHPC to crack initiation under mechanical loading. To further investigate the crack propagation characteristics of the material, this section concentrates on the unstable fracture toughness, denoted as K_{Ic}^{un} in MPa · $m^{1/2}$. The calculation of unstable fracture toughness commences with the determination of $CMOD_c$, as described by Eqs. (4) and (5) [43]:

$$CMOD_c = \frac{24P\max}{BDE} v(\alpha) \tag{4}$$

$$v(\alpha) = 0.76 - 2.28\alpha + 3.87\alpha^2 - 2.04\alpha^3 + \frac{0.66}{(1-\alpha)^2} \tag{5}$$

where P_{max} represents the maximum load (N), while B, D, and E denote the thickness (mm), height (mm), and elastic modulus (MPa) of the DUHPC specimens, respectively. The term $v(\alpha)$ corresponds to the geometric factor, where α is defined as $\alpha = (a + h_0/D + h_0)$ with a denoting the initial crack length and h_0 set to 3 mm, as established in Refs. [48,49].

After calculating the $CMOD_c$, the next step involves determining the critical equivalent fracture length (a_c, mm), which can be calculated using Eq. (6) [50]:

$$a_c = \frac{2}{\pi}(D + h_0)\arctan\sqrt{\frac{BE \times CMOD_c}{32.6P\max} - 0.1135} - h_0 \tag{6}$$

P_{max} and a_c are substituted into Eq. (2) to calculate the unstable fracture toughness K_{Ic}^{un} using Eq. (7):

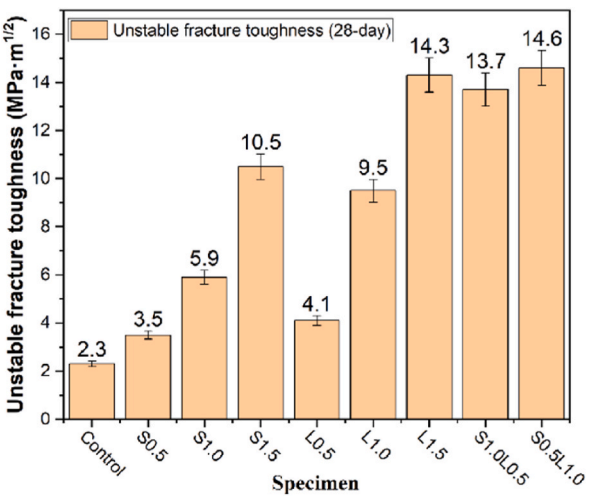

Fig. 8. Unstable fracture toughness of DUHPC specimens after 28 days of curing.

$$K_{Ic}^{un} = \frac{3P_{max}S}{2D^2B}\sqrt{a_c}F\left(\frac{a_c}{D}\right) \quad (7)$$

where S denotes the span length of the DUHPC specimens and $F\left(\frac{a_c}{D}\right)$ is the geometric factor (where a_c substitutes a_0 in Eq. (3)). Fig. 8 illustrates the unstable fracture toughness of steel fibre-reinforced DUHPC after 28 days of curing. The addition of steel fibres significantly enhanced the unstable fracture toughness as compared to the control group. For mono fibre-reinforced DUHPC specimens, the toughness reached its highest value of 14.3 MPa $\cdot$ m$^{1/2}$ when 1.5% of 13 mm steel fibres were incorporated, representing a 521.7% increase compared to the control group, which had a value of 2.3 MPa $\cdot$ m$^{1/2}$. For hybrid DUHPC specimens, although shorter steel fibres replaced partial 13 mm ones in specimen S0.5L1.0, its unstable fracture toughness still slightly increased to 14.6 MPa$\cdot$ m$^{1/2}$, as compared to 14.3 MPa $\cdot$ m$^{1/2}$ in specimen L1.5. This improvement was attributed to the synergistic toughening effect of fibres with different lengths. Furthermore, compared to the initial fracture toughness displayed in Fig. 7, the unstable fracture toughness of DUHPC exhibited a significant enhancement, demonstrating the material's enhanced resistance to crack propagation during unstable fracture stage. Table 5 summarises the increase in unstable relative to initial fracture toughness. From the table, it can be observed that fibre length is a key factor influencing the magnitude of the increase rate in mono fibre-reinforced DUHPC. For example, at a fibre content of 0.5%, the increment was 59.1% for specimen S0.5 and 64.0% for specimen L0.5. When the fibre content increased to 1.0%, the increment was 51.3% for specimen S1.0 and 55.7% for specimen L1.0. This was attributed to the fact that longer fibres provided a stronger bridging effect, extending the fibre pull-out path in the unstable crack propagation stage, enhancing energy dissipation, and thus improving DUHPC resistance to continued crack development. It can also be observed that in hybrid cases, the increment in unstable fracture toughness ranged from 40% to 50.5%, with specimen S0.5L1.0 demonstrating a 40.0% enhancement, slightly lower than the 41.6% observed in specimen L1.5. At the same time, the unstable fracture toughness of specimen S1.0L0.5 was between specimens S1.5 and L1.5.

4.5. Fracture energy

Fracture energy represents another significant mechanical property of fibre-reinforced DUHPC, reflecting the material's ability to absorb energy per unit area of fracture. The fracture energy (G_f, J/ m^2) of DUHPC in a three-point bending test is calculated by Eq. (8):

$$G_f = \frac{W_0 + mgd_0}{A_{lig}} \quad (8)$$

where W_0 is the external work (N·mm), m is the mass of the specimen (kg), g is the gravity acceleration (9.81 m/ s^2), d_0 is the deflection at failure, and A_{lig} is the ligament area (mm^2).

Fig. 9 illustrates the fracture energy of steel fibre-reinforced DUHPC after 28 days of curing. It can be observed that the fracture energy of DUHPC increased with an increase in both the fibre content and length. For example, the fracture energy of specimen S1.0 was 14.3 kJ/ m^2, representing a 64.3% increase as compared to specimen S0.5 of 8.7 kJ/ m^2. When the fibre content increased to 1.5%, specimen S1.5 exhibited an enhancement of 187.2% and 74.7% in comparison with cases S0.5 and S1.0, respectively. This phenomenon was primarily attributed to the increase in steel fibre content, which significantly increased the number of fibres within the crack path. During crack propagation, fibres dissipated substantial energy through pull-out and slip mechanisms, which became a critical factor in enhancing fracture energy. In terms of fibre length, when the fibre content was the same, longer fibres provided higher fracture energy. For instance, the fracture energy of specimen L0.5 was 46.6% higher than S0.5, when the fibre content reached 1.0% and 1.5%, the fracture energy of 13 mm steel fibre-reinforced DUHPC increased by 64.1% and 56.5%, as compared to that of the 10 mm counterparts.

For hybrid fibre-reinforced DUHPC, when 10 mm steel fibres partially replaced 13 mm ones, the fracture energy of DUHPC reduced to a certain extent. Specifically, the energy of specimen S1.0L0.5 decreased by 26.3% as compared to L1.5, while that of specimen S0.5L1.0 decreased by 4.8%. The reason for this phenomenon was that the 10 mm steel fibres had a shorter effective anchorage distance within the matrix, which rendered them more easily pulled out during crack propagation and unable to effectively restrain the continued development of larger cracks. In addition, the reduction in the amount of 13 mm fibres weakened positive effect in providing

Table 5
Increase rate in unstable relative to initial fracture toughness of DUHPC.

Specimens	Initial fracture toughness (MPa$\cdot$ m$^{1/2}$)	Unstable fracture toughness (MPa$\cdot$ m$^{1/2}$)	Increase rate (%)
Control	1.8	2.3	27.7
S0.5	2.2	3.5	59.1
S1.0	3.9	5.9	51.3
S1.5	7.5	10.5	40.0
L0.5	2.5	4.1	64.0
L1.0	6.1	9.5	55.7
L1.5	10.1	14.3	41.6
S0.5L1.0	10.5	14.6	40.0
S1.0L0.5	9.1	13.7	50.5

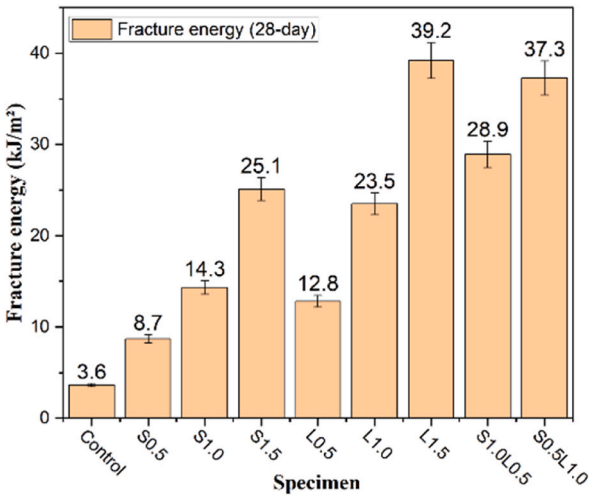

Fig. 9. Fracture energy of DUHPC specimens after 28 days of curing.

effective bridging for bending cracks, which resulted in varying degrees of reduction in the fracture energy of hybrid fibre-reinforced DUHPC.

Table 6 summarises the fracture energy of some representative fibre-reinforced RCC, and self-compacting UHPC with various fibre types, lengths, and contents. Specifically, Karadelis et al. [19] studied the effects of 35 mm straight steel fibres and 50 mm hooked-end steel fibres on RCC. The results demonstrated that, at a fibre content of 1.5%, these two types of steel fibres increased fracture energy to 18.6 kJ/m^2 and 28.3 kJ/m^2, respectively. The research conducted by Wille et al. [51] indicated that when using 3.0% of 30 mm hooked steel fibre, the fracture energy of UHPC showed a notable increase, reaching a maximum of 30.2 kJ/m^2. Dehghanpour et al. [52] reported that incorporating 2.0% of 12 mm steel fibres resulted in a fracture energy of 20.3 kJ/m^2. Similarly, Rojas et al. [53] demonstrated that adding 1.0% and 2.0% of 13 mm steel fibres enhanced UHPC's fracture energy to 16.3 kJ/m^2 and 22.6 kJ/m^2, respectively. It can be noted from the table that the fracture energy of steel fibre-reinforced DUHPC is significantly higher than the reported RCC and UHPC at the same or lower fibre content. Specifically, the fracture energy of the specimen with 13 mm fibres at a content of 1.5% reached 39.2 kJ/m^2. As mentioned in the Introduction and Section 2.2, although RCC likewise employed a similar horizontal rolling casting process, DUHPC also gained from the inherent advantages of UHPC, such as its ultra-high strength and exceptional toughness. Meanwhile, the distribution of fibres in DUHPC matrix showed a distinct variation from the random distribution in self-compacting UHPC. In DUHPC, most steel fibres were aligned parallel to the casting surface, rendering this arrangement effectively enhance the bending load capacity of steel fibre-reinforced DUHPC.

4.6. DIC strain mapping analysis

To precisely monitor the propagation of cracks at the notched site in fibre-reinforced DUHPC specimens, the digital image correlation (DIC) technique was utilized. Fig. 10 illustrates the strain mapping of DUHPC reinforced with 13 mm steel fibres subjected to approximately 90% of the peak load. When the fibre volume content was 0.5%, the primary crack region exhibited noticeable extent, as indicated by the green, yellow, and red areas, with the tensile strain being highly localised within the red and yellow regions. As the fibre content increased to 1.5%, the primary crack region of the specimen significantly diminished in size, and the localisation of tensile strain also weakened. Additionally, the maximum tensile strain observed in the L0.5 specimen was 0.039, noticeably higher than the 0.032 recorded in the L1.5 specimen. This phenomenon can mainly be attributed to the increased fibre content, which resulted in a higher number of fibres at the notch of the specimen and a denser fibre distribution. Consequently, this significantly mitigated the bending deformation of the specimen under the applied load.

Fig. 11 shows the strain mapping of DUHPC reinforced with 10 mm and 13 mm steel fibres at equal fibre content, under approximately 90% of the peak load. When the steel fibre length was 10 mm, the primary crack region of the specimen was visibly wider and longer, exhibiting a higher concentration of tensile strain. Moreover, microcracks prominently extended towards the load application point at the notch of the specimen. In contrast, the main crack region in the L1.0 specimen was smaller, and deformation in the tensile strain region was significantly mitigated. At this load state, the maximum tensile strain for S1.0 specimen was 0.043, slightly higher than the 0.034 observed in L1.0. The DIC strain mapping images corroborated the earlier analyses, confirming that longer steel fibres provide superior strength and toughening effects.

Fig. 12 displays the strain mapping of hybrid fibre-reinforced DUHPC under approximately 90% of the peak load. In specimen S0.5L1.0, the main crack region was noticeably smaller as compared to specimen S1.0L0.5, and the tensile strain region exhibited enhanced performance. Additionally, the maximum strain at the notch in S0.5L1.0 was 0.028, which was lower than the 0.030 observed in specimen S1.0L0.5. Furthermore, compared to L1.5 illustrated in Fig. 10, both the primary crack and tensile strain regions in specimen S0.5L1.0 were significantly optimised. This enhancement can be attributed to the synergistic advantages derived from the

Table 6
Comparison of fracture energy of fibre-reinforced RCC, UHPC, and DUHPC.

References	Concrete	Fibre type	Fibre length (mm)	Fibre content (%)	G_f (kJ/ m^2)
Karadelis et al. [19]	RCC	Straight, hooked	35, 50	1.5	~28.3
Wille et al. [51]	UHPC	Straight, hooked, twisted	13, 30, 18	1.5, 2.0, 2.5, 3.0	~30.2
Dehghanpour [52].	UHPC	Straight	12	0.7, 1.3, 2.0	~20.3
Rojas et al. [53]	UHPC	Straight	13	1.0, 2.0	~22.6
This study	DUHPC	Straight	10, 13	0.5, 1.0, 1.5	~39.2

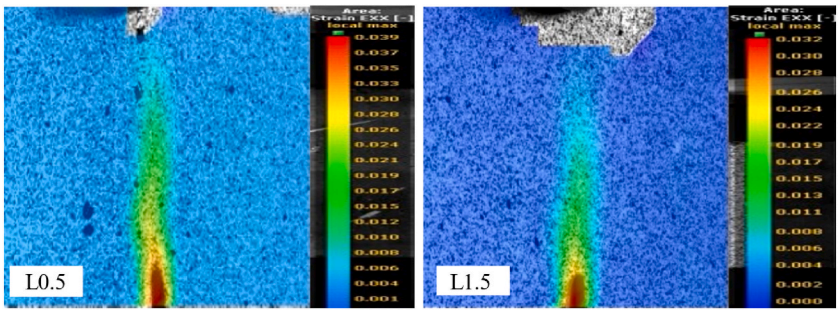

Fig. 10. Strain mapping of 13 mm steel fibre-reinforced DUHPC at contents of 0.5% and 1.5%.

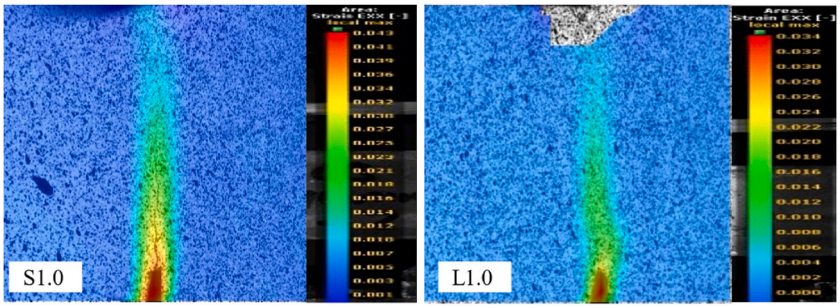

Fig. 11. Strain mapping of 10 mm and 13 mm steel fibre-reinforced DUHPC at a content of 1.0%.

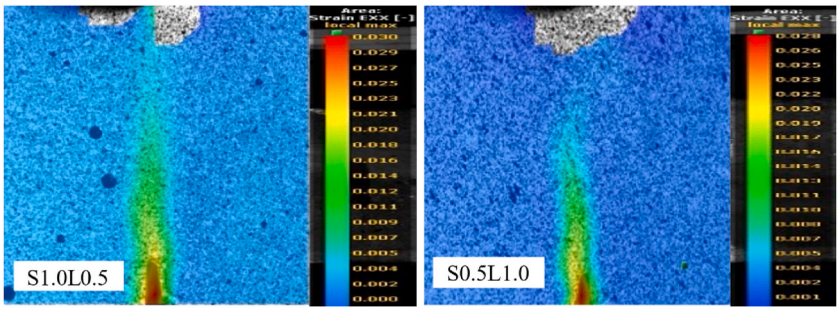

Fig. 12. Strain mapping of hybrid steel fibre-reinforced DUHPC at a content of 1.5%.

combination of steel fibres of varying lengths, which optimally balanced both the fibre quantity and length.

4.7. SEM analysis

The scanning electron microscope (SEM) plays a crucial role in the analysis of fibre-reinforced concrete via providing the high-resolution insights into the material's microstructural patterns. Fig. 13 presents the SEM images of the steel fibre-reinforced DUHPC. The DUHPC matrix exhibited remarkable densification, primarily due to the early application of the moderate high-temperature moist/steam curing followed by stable water curing. This treatment promoted the formation of abundant gel phases

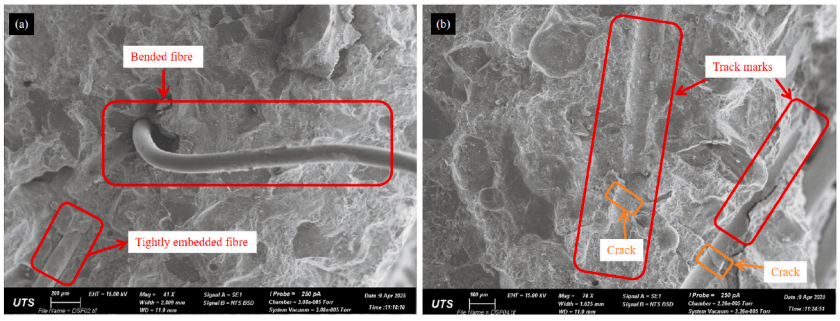

Fig. 13. SEM micrographs of steel fibre-reinforced DUHPC.

that effectively filled the matrix pores. As shown in Fig. 13(a), the steel fibre exhibited pronounced bending at its anchorage point within the matrix, reflecting a high interfacial bond strength that beneficial for delaying crack propagation and dissipating energy under loads. Residual cement paste adhering to the steel fibre surface further confirmed its robust interfacial bonding with the surrounding matrix prior to deformation. In addition, the steel fibre located at the lower left corner of the image was observed to be tightly embedded within the adjacent matrix, providing additional evidence of excellent fibre-matrix adhesions. Furthermore, the traces observed in Fig. 13(b) revealed distinct track marks left behind after the fibre pull-out, further confirming that the fibres enhanced flexural performance not only through deformation but also via frictional resistance along the fibre-matrix interface. Such pull-out property is particularly beneficial, as it facilitates progressive energy dissipation and mitigates sudden failure. Cracks were also noted at the bottom of the track marks. This phenomenon is consistent with the observations reported by Jiao et al. [54], indicating that the steel fibres carried substantial stress during the initial stages of loading until they were fully pulled out and the specimen ultimately fractured. Overall, these findings demonstrate that the embedded steel fibres significantly improve the material's resistance to bending loads through the synergistic effects of fibre deformation, pull-out, and interfacial friction, thereby enhancing the overall flexural performance of DUHPC.

5. Conclusions and future work

This study experimentally investigates the effect of mono and hybrid steel fibres on DUHPC flexural behaviour, including the load-CMOD relationship, strength, initial fracture toughness, unstable fracture toughness, and fracture energy. Additionally, DIC and SEM techniques were employed to examine the failure patterns and microstructural characteristics of DUHPC. Based on the analysis and discussion, the following key findings can be concluded.

1) The load-CMOD relationships indicated that the length and content of steel fibres had a significant impact on the peak load and CMOD behaviour of DUHPC. Longer and higher content of steel fibres can provide a greater peak load and higher residual load-carrying capacity at the same CMOD. The post-peak fluctuations observed in the curves of hybrid fibre specimens were attributed to the progressive pull out of shorter fibres, while longer ones continued to restrain the cracks.
2) For mono fibre-reinforced DUHPC, flexural strength, initial fracture toughness, unstable fracture toughness, and fracture energy notably increased as the fibre length and content increased. At 28 days of curing, the strength of DUHPC incorporating 1.5% 13 mm steel fibres peaked at 36.1 MPa. Additionally, as compared to 10 mm fibres, the initial fracture toughness and energy were enhanced by 34.7% and 56.5%, respectively, and the unstable fracture toughness was enhanced by 36.2%.
3) For hybrid fibre reinforcement, partially replacing 13 mm fibres with shorter ones resulted in varying degrees of reduction in both flexural strength and fracture energy as compared to specimen L1.5. However, the initial and unstable fracture toughness improved by 3.9% and 2.1%, respectively, which is attributed to the synergistic effect of fibres with different lengths and a reduced likelihood of agglomeration of longer steel fibres within the concrete matrix.
4) DIC strain mapping demonstrated that longer steel fibres substantially reduced the primary crack region and strain localisation. However, shorter fibres, particularly at lower contents, exhibited a limited capacity to restrain the fibre propagation and specimen deformation. Hybrid fibre reinforcements optimised both the major crack region and strain localisation, benefiting from the synergistic effects of steel fibres of varied lengths.
5) SEM micrographs revealed that the high-temperature moist/steam curing used for DUHPC promoted the gel formation, effectively filling the pores within the matrix and resulting in a significantly denser microstructure. Meanwhile, the deformation and tight embedding of steel fibres demonstrated excellent fibre-matrix adhesion. Furthermore, the distinct traces observed after fibre pull-out confirmed that the fibres improved flexural performance not only through deformation but also via frictional resistance along the fibre-matrix interface.

Extensive research on the static performance of fibre-reinforced DUHPC has primarily focused on steel reinforcements, while the potential of plant fibres as sustainable alternatives has not been thoroughly investigated. A promising approach could involve replacing steel with plant fibres to enhance sustainability. Additionally, although UHPC is well-established in structural engineering,

the adoption of DUHPC in practical settings remains limited. Future research will explore the performance of DUHPC reinforced with various types of plant fibres under diverse environmental conditions. Further investigations will also evaluate DUHPC performance when reinforced with steel and plant fibres. The studies will extend to applications such as roof tiles and lightweight precast elements, focusing on enhancing workability, manufacturing processes, structural integrity, and static and dynamic mechanical properties to improve cost-effectiveness and sustainability, as well as facilitate construction.

CRediT authorship contribution statement

Chaocong Wang: Writing – original draft, Methodology, Investigation, Formal analysis. **Ruizhe Shao:** Writing – review & editing, Supervision, Methodology, Conceptualization. **Jianguang Fang:** Writing – review & editing, Supervision, Methodology, Conceptualization. **Jun Li:** Writing – review & editing, Resources, Conceptualization. **Chengqing Wu:** Writing – review & editing, Supervision, Resources, Methodology, Conceptualization.

Declaration of competing interest

The authors declare that they have no known competing financial interests or personal relationships that could have appeared to influence the work reported in this paper.

Acknowledgement

This study was funded by ARC Discovery Grant DP210101100. Acknowledgments go to Junjie Huang and Zizheng Yu for their help with the experimental work.

Data availability

Data will be made available on request.

References

[1] A.C. Institute, Guide for Selecting Proportions for No Slump Concrete, 211.3 R-02, ACI, Farmington Hills, MI, 2002, pp. 1–26.
[2] C.D. Burns, K.L. Saucier, Vibratory compactation study of zero-slump concrete, Journal Proceedings (1978) 753.
[3] T.-C. Ling, Effects of compaction method and rubber content on the properties of concrete paving blocks, Constr. Build. Mater. 28 (1) (2012) 164–175.
[4] A. Aghaeipour, M. Madhkhan, Mechanical properties and durability of roller compacted concrete pavement (RCCP)–a review, Road Mater. Pavement Des. 21 (7) (2020) 1775–1798.
[5] P. Sukontasukkul, C. Chaikaew, Properties of concrete pedestrian block mixed with crumb rubber, Constr. Build. Mater. 20 (7) (2006) 450–457.
[6] C. Chhorn, S.J. Hong, S.-W. Lee, A study on performance of roller-compacted concrete for pavement, Constr. Build. Mater. 153 (2017) 535–543.
[7] S. Chidiac, S. Mihaljevic, Performance of dry cast concrete blocks containing waste glass powder or polyethylene aggregates, Cement Concr. Compos. 33 (8) (2011) 855–863.
[8] D. Harrington, F. Abdo, H. Ceylan, W. Adaska, C. Hazaree, F. Bektas, Guide for roller-compacted Concrete Pavements, 2010.
[9] D.W. Pittman, Construction of roller-compacted concrete pavements, Transp. Res. Rec. 1062 (1986) 13–19.
[10] I. Kett, Engineered Concrete: Mix Design and Test Methods, CRC Press, 2009.
[11] R. Shao, C. Wu, J. Li, A comprehensive review on dry concrete: application, raw material, preparation, mechanical, smart and durability performance, J. Build. Eng. 55 (2022) 104676.
[12] A.A. Ramezanianpour, A. Mohammadi, E.R. Dehkordi, Q.B. Chenar, Mechanical properties and durability of roller compacted concrete pavements in cold regions, Constr. Build. Mater. 146 (2017) 260–266.
[13] S. Ghahari, A. Mohammadi, A. Ramezanianpour, Performance assessment of natural pozzolan roller compacted concrete pavements, Case Stud. Constr. Mater. 7 (2017) 82–90.
[14] A.A. Al-Tameemi, K.M. A'mina, Influence of polypropylene fibers reinforcement on the mechanical properties of roller compacted concrete used in airports with partial replacement of cement by cement kiln dust, J. Phys. Conf. (2021) 19731.
[15] A. Peyvandi, P. Soroushian, Structural performance of dry-cast concrete nanocomposite pipes, Mater. Struct. 48 (2015) 461–470.
[16] A. Peyvandi, P. Soroushian, A.M. Balachandra, K. Sobolev, Enhancement of the durability characteristics of concrete nanocomposite pipes with modified graphite nanoplatelets, Constr. Build. Mater. 47 (2013) 111–117.
[17] Ş. Yazici, A. Mardani-Aghabaglou, M. Tuyan, A.A. Üte, Mechanical properties and impact resistance of roller-compacted concrete containing polypropylene fibre, Mag. Concr. Res. 67 (16) (2015) 867–875.
[18] H. Rooholamini, A. Hassani, M. Aliha, Fracture properties of hybrid fibre-reinforced roller-compacted concrete in mode I with consideration of possible kinked crack, Constr. Build. Mater. 187 (2018) 248–256.
[19] J.N. Karadelis, Y. Lin, Flexural strengths and fibre efficiency of steel-fibre-reinforced, roller-compacted, polymer modified concrete, Constr. Build. Mater. 93 (2015) 498–505.
[20] P. Sukontasukkul, U. Chaisakulkiet, P. Jamsawang, S. Horpibulsuk, C. Jaturapitakkul, P. Chindaprasirt, Case investigation on application of steel fibers in roller compacted concrete pavement in Thailand, Case Stud. Constr. Mater. 11 (2019) e00271.
[21] J. LaHucik, S. Dahal, J. Roesler, A.N. Amirkhanian, Mechanical properties of roller-compacted concrete with macro-fibers, Constr. Build. Mater. 135 (2017) 440–446.
[22] M.K. Sharbatdar, F. Rahmati, Experimental evaluation of multi-functional effects of fibers on mechanical and performance properties of roller-compacted concrete pavements (RCCP), Constr. Build. Mater. 316 (2022) 125890.
[23] D. Scorza, R. Luciano, S. Mousa, S. Vantadori, Fracture behaviour of hybrid fibre-reinforced roller-compacted concrete used in pavements, Constr. Build. Mater. 271 (2021) 121554.
[24] N. Liang, R. Yan, Q. Miao, G. Cao, X. Liu, Effect of multi-scale polypropylene fiber hybridization on compressive constitutive mechanics parameters of roller compacted concrete, Struct. Concr. 23 (1) (2022) 441–456.
[25] M. Bajaber, I. Hakeem, UHPC evolution, development, and utilization in construction: a review, J. Mater. Res. Technol. 10 (2021) 1058–1074.
[26] Q. Luo, Y.-Y. Wu, W. Qiu, H. Huang, S. Pei, P. Lambert, D. Hui, Improving flexural strength of UHPC with sustainably synthesized graphene oxide, Nanotechnol. Rev. 10 (1) (2021) 754–767.

[27] H. Zhang, T. Ji, X. Zeng, Z. Yang, X. Lin, Y. Liang, Mechanical behavior of ultra-high performance concrete (UHPC) using recycled fine aggregate cured under different conditions and the mechanism based on integrated microstructural parameters, Constr. Build. Mater. 192 (2018) 489–507.
[28] Y. Kusumawardaningsih, E. Fehling, M. Ismail, UHPC compressive strength test specimens: cylinder or cube? Procedia Eng. 125 (2015) 1076–1080.
[29] R. Shao, C. Wu, J. Li, Z. Liu, Development of sustainable steel fibre-reinforced dry ultra-high performance concrete (DUHPC), J. Clean. Prod. 337 (2022) 130507.
[30] R. Shao, C. Wu, J. Li, Z. Liu, P. Wu, Y. Yang, Mechanical behaviour and environmental benefit of eco-friendly steel fibre-reinforced dry UHPC incorporating high-volume fly ash and crumb rubber, J. Build. Eng. 65 (2023) 105747.
[31] R. Shao, C. Wu, J. Li, Z. Liu, Investigation on the mechanical characteristics of multiscale mono/hybrid steel fibre-reinforced dry UHPC, Cement Concr. Compos. 133 (2022) 104681.
[32] L. Hebda, L. Rudzinski, B. Turlej, Optimizing the Composition of Polypropylene Fibre Reinforced Cementitious Composites, Fibre Reinforced Cement and Concrete, CRC Press, 1992, pp. 357–365.
[33] Y. Rui, L. Kangning, Y. Tianyi, T. Liwen, D. Mengxi, S. Zhonghe, Comparative study on the effect of steel and polyoxymethylene fibers on the characteristics of ultra-high performance concrete (UHPC), Cement Concr. Compos. 127 (2022) 104418.
[34] H. Fang, M. Gu, S. Zhang, H. Jiang, Z. Fang, J. Hu, Effects of steel fiber and specimen geometric dimensions on the mechanical properties of ultra-high-performance concrete, Materials 15 (9) (2022) 3027.
[35] D.-Y. Yoo, Y.-S. Yoon, N. Banthia, Flexural response of steel-fiber-reinforced concrete beams: effects of strength, fiber content, and strain-rate, Cement Concr. Compos. 64 (2015) 84–92.
[36] D.-Y. Yoo, S.-T. Kang, Y.-S. Yoon, Enhancing the flexural performance of ultra-high-performance concrete using long steel fibers, Compos. Struct. 147 (2016) 220–230.
[37] Y. Zhang, Y. Zhu, S. Qu, A. Kumar, X. Shao, Improvement of flexural and tensile strength of layered-casting UHPC with aligned steel fibers, Constr. Build. Mater. 251 (2020) 118893.
[38] C. Magureanu, I. Sosa, C. Negrutiu, B. Heghes, Physical and mechanical properties of ultra high strength fiber reinforced cementitious composites, Fracture Mechanics of Concrete and Concrete Structures, Korea Concrete Institute (2010).
[39] M. Shafieifar, M. Farzad, A. Azizinamini, Experimental and numerical study on mechanical properties of ultra high performance concrete (UHPC), Constr. Build. Mater. 156 (2017) 402–411.
[40] Z. Wu, C. Shi, W. He, L. Wu, Effects of steel fiber content and shape on mechanical properties of ultra high performance concrete, Constr. Build. Mater. 103 (2016) 8–14.
[41] P. Maca, R. Sovjak, T. Vavřiník, Experimental investigation of mechanical properties of UHPFRC, Procedia Eng. 65 (2013) 14–19.
[42] M.L.d. Silva, L.P. Prado, E.F. Félix, A.M.D.d. Sousa, D.P. Aquino, The influence of materials on the mechanical properties of ultra-high-performance concrete (UHPC): a literature review, Materials 17 (8) (2024) 1801.
[43] Y. Wang, S. Hu, X. Sun, Experimental investigation on the elastic modulus and fracture properties of basalt fiber–reinforced fly ash geopolymer concrete, Constr. Build. Mater. 338 (2022) 127570.
[44] Y. Niu, J. Wei, C. Jiao, Multi-scale fiber bridging constitutive law based on meso-mechanics of ultra high-performance concrete under cyclic loading, Constr. Build. Mater. 354 (2022) 129065.
[45] S.-Y. Fu, Y.-W. Mai, B. Lauke, C.-Y. Yue, Synergistic effect on the fracture toughness of hybrid short glass fiber and short carbon fiber reinforced polypropylene composites, Mater. Sci. Eng., A 323 (1–2) (2002) 326–335.
[46] Z.-W. Cai, J.-T. Yu, X.-Z. Duan, B.-Y. Deng, Z.-D. Lu, K.-Q. Yu, Enhancing the strain-hardening performance of ultra-high performance concrete by tailoring matrix toughness and fiber parameters, Constr. Build. Mater. 395 (2023) 132335.
[47] L. Yu, S. Bai, X. Guan, Effect of multi-scale reinforcement on fracture property of ultra-high performance concrete, Constr. Build. Mater. 397 (2023) 132383.
[48] H. Tada, P.C. Paris, G.R. Irwin, The Stress Analysis of Cracks, Handbook, Del Research Corporation, 1973, p. 34, 1973.
[49] S. Xu, H.W. Reinhardt, Determination of double-K criterion for crack propagation in quasi-brittle fracture, Part I: experimental investigation of crack propagation, Int. J. Fract. 98 (2) (1999) 111–149.
[50] Y. Liu, J. Xie, J.-B. Yan, Flexural and fracture performance of UHPC exposed to low-temperature environment, Constr. Build. Mater. 373 (2023) 130865.
[51] K. Wille, S. El-Tawil, A.E. Naaman, Properties of strain hardening ultra high performance fiber reinforced concrete (UHP-FRC) under direct tensile loading, Cement Concr. Compos. 48 (2014) 53–66.
[52] H. Dehghanpour, S. Subasi, S. Guntepe, M. Emiroglu, M. Marasli, Investigation of fracture mechanics, physical and dynamic properties of UHPCs containing PVA, glass and steel fibers, Constr. Build. Mater. 328 (2022) 127079.
[53] R. Rojas, J.R. Yepez, C. Américo Filho, Numerical simulation of beams manufactured with ultra-high performance fibre reinforced concrete (UHPFRC), in: XL Ibero-Latin American Congress on Computational Methods in Engineering, 2019, p. 101.
[54] Y. Jiao, Y. Zhang, M. Guo, L. Zhang, H. Ning, S. Liu, Mechanical and fracture properties of ultra-high performance concrete (UHPC) containing waste glass sand as partial replacement material, J. Clean. Prod. 277 (2020) 123501.